Effects of Deletion and Site-Directed Mutations on Ligation Steps of NAD^+-Dependent DNA Ligase: A Biochemical Analysis of BRCA1 C-Terminal Domain†

Hong Feng,‡ Jeremy M. Parker,‡ Jing Lu, and Weiguo Cao*

Department of Genetics, Biochemistry & Life Science Studies, South Carolina Experiment Station, Clemson University, Room 219, Biosystems Research Complex, 51 New Cherry Street, Clemson, South Carolina 29634

Received March 19, 2004; Revised Manuscript Received June 18, 2004

ABSTRACT: DNA strand joining entails three consecutive steps: enzyme adenylation to form AMP−ligase, substrate adenylation to form AMP−DNA, and nick closure. In this study, we investigate the effects on ligation steps by deletion and site-directed mutagenesis of the BRCA1 C-terminal (BRCT) domain using NAD^+-dependent DNA ligase from *Thermus* species AK16D. Deletion of the BRCT domain resulted in substantial loss of ligation activity, but the mutant was still able to form an AMP−ligase intermediate, suggesting that the defects caused by deletion of the entire BRCT domain occur primarily at steps after enzyme adenylation. The lack of AMP−DNA accumulation by the domain deletion mutant as compared to the wild-type ligase indicates that the BRCT domain plays a role in the substrate adenylation step. Gel mobility shift analysis suggests that the BRCT domain and helix−hairpin−helix subdomain play a role in DNA binding. Similar to the BRCT domain deletion mutant, the G617I mutant showed a low ligation activity and lack of accumulation of AMP−DNA intermediate. However, the G617I mutant was only weakly adenylated, suggesting that a point mutation in the BRCT domain could also affect the enzyme adenylation step. The significant reduction of ligation activity by G634I appears to be attributable to a defect at the substrate adenylation step. The greater ligation of mismatched substrates by G638I is accountable by accelerated conversion of the AMP−DNA intermediate to a ligation product at the final nick closure step. The mutational effects of the BRCT domain on ligation steps in relation to protein−DNA and potential protein−protein interactions are discussed.

DNA ligases are essential components of DNA replication, repair, and recombination; and they catalyze the phosphodiester bond formation of single-stranded nicks in double-stranded DNA (*1*). DNA ligases can be classified into two categories based on their need for either NAD^+ or ATP. ATP-dependent DNA ligases are present in various organisms, such as mammals and yeast, viruses, Archaea, bacteriophages, and eubacteria (*2*). However, NAD^+-dependent ligases are initially found in eubacteria and later in some entomopoxviruses (*2*). Regardless of the choice of the adenylation cofactor, a reaction catalyzed by DNA ligase requires three distinct steps. First, adenylation of the ϵ-lysine present within the essential KXDG motif of the adenylation domain in ligases occurs via the adenylate portion of an NAD^+ molecule. Second, the adenylate moiety is then transferred to the 5′-terminal phosphate present at the nick. The third and final step involves phosphodiester bond formation via a nucleophilic attack of the 3′-hydroxy terminus present at the other side of the nick (*1*).

Both ATP- and NAD^+-dependent DNA ligases belong to a nucleotidyl transferase superfamily, the members of which also include RNA ligases and RNA capping enzymes (*2*−*5*). The common structural feature of this superfamily is that each member contains a nucleotidyl transferase core that consists of six conserved motifs. Extensive biochemical and structural studies have defined the role of some of these motifs in multiple nucleotidyl transfer reactions (*3*, *6*−*24*). Bacterial NAD^+-dependent DNA ligases contain an adenylation domain at the N-terminus followed by an OB-fold domain, a zinc finger, a four-helix−hairpin−helix-motif (HhH) domain, and a BRCT[1] domain (Figure 1). NAD^+-dependent DNA ligases found in entomopoxviruses and some second NAD^+-dependent DNA ligases found in bacteria, however, do not contain the C-terminal BRCT domain (*12*, *14*).

The BRCT domain was originally identified as a small domain in proteins involved in cell cycle control and DNA

† This work was supported in part by CSREES/USDA (Grant SC-1700153, technical contribution No. 4974), NIH (Grants CA65930 and GM067744), and a Howard Hughes Medical Institute Undergraduate Internship.

* To whom correspondence should be addressed. Tel: (864) 656-4176. Fax: (864) 656-0393. E-mail: wgc@clemson.edu.

‡ Contributed equally to this work.

[1] Abbreviations: AMP, adenosine 5′-monophosphate; *Apy*, *Aquifex pyrophilus*; ATP, adenosine 5′-triphosphate; BRCT, BRCA1 C-terminal domain; BSA, bovine serum albumin; *Bst*, *Bacillus stearothermophilus*; dNTP, deoxyribonucleoside triphosphate; DTT, dithiothreitol; IPTG, isopropyl-β-D-thiogalactopyranoside; NAD^+, nicotinamide adenine dinucleotide; NMN, nicotinamide mononucleotide; OB-fold, oligonucleotide/oligosaccharide binding fold; PMSF, phenylmethanesulphonyl fluoride; PPi, pyrophosphate; *Sau*, *Staphylococcus aureus*; *Tfi*, *Thermus filiformis*; Tsp, *Thermus* species; wt, wild-type.

10.1021/bi049451c CCC: $27.50
Published on Web 09/11/2004

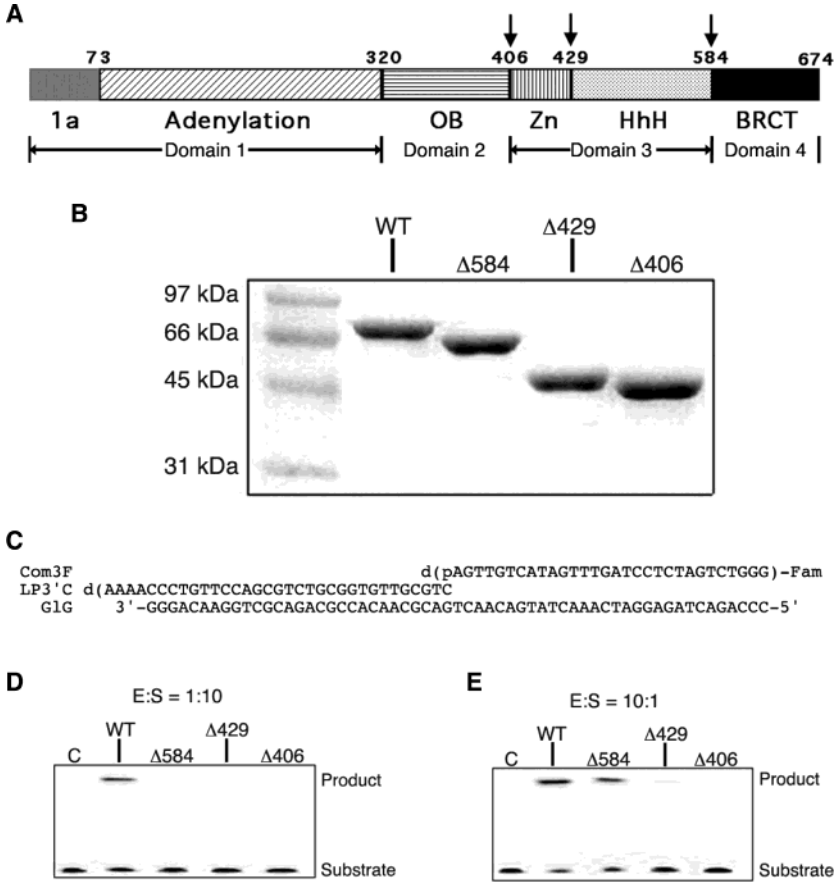

FIGURE 1: Domain deletion in Tsp AK16D DNA ligase. Panel A presents the domain organization of Tsp AK16D DNA ligase: 1a (gray), subdomain 1a; Adenylation (diagonal lines), adenylation subdomain; OB (horizontal lines), OB fold; Zn (vertical lines), Zn finger; HhH (crosshatch), helix−hairpin−helix motifs; BRCT (black), BRCT domain. Sites of deletion mutations are marked with an arrow. Panel B shows SDS−PAGE analysis of purified deletion mutants. Purified deletion mutant proteins were analyzed on a 15% SDS−PAGE gel and visualized using Coomassie brilliant blue staining. Panel C shows the perfectly matched nicked substrate. Panel D shows the ligation activity of deletion mutants with E/S (enzyme/substrate) ratio = 1:10. Reactions mixtures (20 μL) containing 20 mM Tris-HCl (pH 7.6), 100 mM KCl, 10 mM dithiothreitol, 20 μg/mL BSA, 10 mM $MgCl_2$, 1 mM NAD^+, 1 nM ligase deletion mutant, and 10 nM nicked C/G substrate were incubated at 65 °C for 30 min and then analyzed on the 10% GeneScan gel. Panel E shows the ligation activity of deletion mutants with E/S = 10:1. The ligation assays were performed identical to those in panel D except that the ligase deletion mutant concentration was increased to 100 nM.

repair ((*25*, *26*). BRCT domains may function as a protein−protein interaction module (*27*−*33*), in DNA binding (*34*−*36*), and in recognition of phosphopeptides (*37*, *38*). Some of the eukaryotic ATP-dependent ligases contain one or tandem BRCT domains (*2*, *39*). Interactions between human ligase IIIa and XRCC1 are mediated by BRCT domains located in both proteins (*30*, *33*, *40*). Previously, we biochemically characterized a high-fidelity ligase from *Thermus* species AK16D (*41*). We herein report domain deletion and site-directed mutagenesis on the Tsp AK16D thermostable DNA ligase. Deletion mutational analysis indicates that the BRCT domain, along with HhH motifs, Zn finger, and OB fold, plays an important role in ligation function. Site-directed mutagenesis performed on conserved residues of the BRCT domain further underscores the functional role of this domain in different steps of strand joining. To the best of our knowledge, this is the first site-directed mutagenesis analysis addressing the relationship between the BRCT domain and the ligation steps.

EXPERIMENTAL PROCEDURES

Reagents, Media, and Strains. Routine chemical reagents were purchased from Sigma (St. Louis, MO), VWR (Suwanee, GA), or Fisher Scientific (Suwanee, GA). Restriction enzymes were obtained from New England Biolabs (Beverly, MA). *Pfu* DNA polymerase and other components of the QuikChange kit were purchased from Stratagene (La Jolla, CA). LB medium was prepared according to standard recipes. Sonication buffer consisted of 20 mM HEPES−KOH (pH 7.2), 0.5 mM DTT, 0.5 mM PMSF, 10% glycerol, 0.5 mM EDTA, and 50 mM NaCl. Ligase activity assay buffer consisted of 20 mM Tris-HCl (pH 7.6), 100 mM KCl, 10 mM DTT, and 20 μg/mL BSA. GeneScan stop solution consisted of 1% Blue Dextran, 80% formamide, and 50 mM EDTA. PBS buffer (pH 7.4) consisted of 137 mM NaCl, 2.7 mM KCl, 10 mM Na_2PO_4, and 2 mM KH_2PO_4. The plasmid pEV5 used for cloning was from our laboratory collections (*42*). *Escherichia coli* BL21(DE3)pLysS cells and plasmid pET11c were obtained from Novagen (Madison, WI). JM109 cells were purchased from Promega (Madison, WI). Hitrap columns were purchased from Amersham Bioscience (Piscataway, NJ). Deoxyribooligonucleotides were ordered from Integrated DNA Technologies (Coralville, IA).

Generation and Purification of Domain Deletion Mutants of Tsp AK16D DNA Ligases. Domain deletions were generated by PCR using the forward primer (Seq22, 5′-GCC

TCG AAA TTC TGT CAT-3′) and one of the reverse primers targeted at different deletion sites (Tak.406R for deleting OB-fold, zinc finger, and BRCT domain, 5′-GCG CCT *GGA TCC CTA* GGG CCA GAT GAT GGG CTT CT-3′; Tak.429R for deleting HhH motifs and BRCT domain, 5′-GCG CCT GGA TCC *CTA* CAA GGG GTT GGG GCA GCG GT-3′; Tak.584R for deleting BRCT domain, 5′-GCG CCT GGA TCC *CTA* TTT GGC CTC CAT CTC CAC CC-3′; the *Bam*HI sites are underlined and the stop codon are italicized). The PCR reaction mixtures (100 μL) consisted of 1 ng of pEV5-Tak, 50 μM each dNTP, 2.5 U of *Taq* DNA polymerase, 0.6 μM forward primer, and 0.6 μM one of the three reverse primers. The PCR procedure was carried out with a predenaturation step at 95 °C for 30 s, 25 cycles of two-step amplification with each cycle consisting of denaturation at 94 °C for 30 s and annealing-extension at 65 °C for 6 min, and a final extension step at 72 °C for 5 min. The PCR products were purified by routine phenol extraction and ethanol precipitation. The purified PCR products and the vector pEV5 were digested with *Nde*I and *Bam*HI and ligated. The ligation products were transformed into *E. coli* strain AK53 by a one-step protocol (*43*). The resulting plasmids, pEV-Tak584, pEV-Tak429, and pEV-Tak406, were sequenced to verify the fidelity of PCR amplification. Fragments containing ligase deletion mutants were subcloned into expression vector pET11c through *Nde*I and *Bam*HI digestion. The resulting plasmids, named as pET-Tak584, pET-Tak429, and pET-Tak406, respectively, were transformed into *E. coli* strain BL21(DE3).

To overexpress the domain deletion mutants of the Tsp AK16D DNA ligase, an overnight culture of *E. coli* strains containing pET-Tak584, pET-Tak429, or pET-Tak406 was diluted 100-fold into 1 L of LB medium supplemented with 0.2% glucose and 50 μg/mL ampicillin. The *E. coli* strain was grown at 37 °C with shaking at 250 rpm until the optical density at 550 nm reached about 0.6. After adding IPTG to a final concentration of 1 mM, the culture was incubated at 37 °C with shaking for another 3.5−4 h to induce protein expression. The induced *E. coli* cells were harvested by centrifugation at 4000 rpm for 10 min, washed with PBS buffer, and stored at −20 °C prior to use.

The *E. coli* cell paste from 1 L of culture was suspended in 10 mL of sonication buffer containing 20 mM Tris-HCl (pH 7.6), 1 mM EDTA, 0.5 mM PMSF, 0.5 mM DTT, and 50 mM NaCl on ice, sonicated at Output 3 for 3 × 30 s using Branson Sonifier 450, and clarified by centrifugation. The supernatant was heated at 70 °C for 30 min to denature *E. coli* proteins and then cooled on ice. Denatured proteins were pelleted by centrifugation at 12 000 rpm for 30 min. The remaining proteins in the heat-treated supernatant were precipitated by adding ammonium sulfate to 80% saturation. The precipitate was collected by centrifugation at 12 000 rpm at 4 °C and dissolved in 10 mL of Butyl buffer A (20 mM Tris-HCl (pH 8.0), 1 mM EDTA, 0.2 mM DTT, 3 M NaCl). The sample was loaded onto a 5 mL HiTrap Butyl FF column, and the proteins were eluted with 6 column volumes (CV) of a descending linear gradient of NaCl (3−0 M) in the same buffer. Fractions containing ligase protein as shown in 15% SDS−PAGE gels (2.10−1.35 M NaCl) were pooled and dialyzed against HiTrap Blue buffer A (20 mM Tris-HCl (pH 8.0), 0.5 mM EDTA, 0.5 mM DTT) overnight in cold room. The sample was clarified by centrifugation and loaded onto a 1 mL HiTrap Blue column. The protein was eluted with 10 CV of an ascending linear gradient of NaCl (0−1 M) in HiTrap Blue buffer. Fractions containing ligase protein (0.35−0.50 M NaCl) were pooled, and protein concentrations were determined by quantifying the intensity of protein bands on a 15% SDS−PAGE gel using BSA as a standard.

Site-Directed Mutagenesis at the BRCT Domain of the Tsp AK16D DNA Ligase. Site-directed mutagenesis was conducted according to the instructional manual of the QuikChange mutagenesis kit (Stratagene). The pEV5-Tak plasmid containing the Tsp AK16D ligase gene was used as the template for initial incorporation of mutant sequences. The mutagenized plasmids were transformed into *E. coli* JM109 competent cells. Plasmids were then isolated using QIAprep plasmid miniprep kit (Qiagen). The entire ligase open reading frame was sequenced to confirm that only a desired site-directed mutation was introduced. A mutation-containing fragment was generated by *Nco*I and *Bam*HI digestion and substituted for the wild-type ligase gene fragment in pET11c-Tak by subcloning. The resulting plasmids were transformed into *E. coli* strain BL21(DE3). Plasmids were isolated and the BRCT domain region was sequenced again to verify the mutations. *E. coli* BL21(DE3) cells containing 13 site-directed mutants were cultured overnight at 37 °C in LB medium containing 50 μg/mL ampicillin. Induction, sonication, partial purification by heat treatment, and protein quantitation were performed as described above.

Substrates and Ligation Assays. The deoxyribooligonucleotide perfectly matched nicked substrate was formed by annealing two short oligonucleotides (33-mer for LP3′C and 30-mer for Com3F) with a 59-mer complementary oligonucleotide (Glg) (Figure 1C). Oligonucleotides LP3′C and Glg were in 1.5-fold excess so that all the 3′ Fam-labeled Com3F represented nicked substrates. A substrate with a mismatch at the 3′-penultimate position of a nick was formed by annealing LP3′C and Com 3′F to the complementary strand (GGlg) (Figure 7). A substrate with a mismatch at the 3′ position of a nick was formed by annealing LP3′T and Com 3′F to the complementary strand (Glg) (Figure 8). The nicked DNA duplex substrates were formed by denaturing DNA at 94 °C for 2 min followed by reannealing at 65°C for 2 min in ligation buffer.

Ligation mixtures (20 μL) containing the indicated amount of DNA ligase, 10 nM 3′-Fam-labeled substrate, 20 mM Tris-HCl (pH 7.6), 100 mM KCl, 10 mM dithiothreitol, 20 μg/mL BSA, 10 mM $MgCl_2$, and 1 mM NAD^+ (unless otherwise stated) were incubated at 65 °C for 30 min. Addition of an equal volume of GeneScan stop solution terminated the reaction. Samples (3.5 μL) were denatured for 3 min at 95 °C prior to separation on an 8 M urea−10% GeneScan gel according to the instructional manual on an ABI PRISM 373XL sequencer or an ABI PRISM 377 sequencer (Applied Biosystems). Results were quantified using GeneScan software (Applied Biosystems).

Enzyme Adenylation Assays. Enzyme adenylation reaction mixtures (10 μL) containing 5 μM ligase protein, 20 mM Tris-HCl (pH 7.6), 50 mM KCl, 5 mM $MgCl_2$, 0.5 mM EDTA, and 0.5 mM [^{32}P]-NAD^+ (1000 Ci/mmol, Amersham Biosciences) were incubated at 65 °C for 30 min. In the case of NAD^+ titration assays, the adenylation assay was under

the same conditions as described above, except that various concentrations of [^{32}P]-NAD$^+$ were added into each separate reaction tube. Reactions were stopped by adding 2× SDS−PAGE loading buffer. Samples were boiled for 5 min and analyzed by 15% SDS−PAGE. Gels were exposed in a phosphorimager screen at −20 °C for about 3 h and then scanned using a Typhoon 9400 phosphorimager (Amersham Biosciences).

Gel Mobility Shift Assays. The gel mobility shift assays were performed as described previously (*44*). The binding reaction mixtures contained 50 nM fluorescently labeled nicked C/G oligonucleotide substrate, 20 mM Tris-HCl (pH 7.6), 1 mM DTT, 15% glycerol, and 4 μM wt or mutant ligase protein. The binding reactions were carried out at room temperature for 30 min. Samples were electrophoresed on a 6% native polyacrylamide gel in 1× TBE buffer. The bound and free DNA species were analyzed using a Typhoon 9400 Imager (Amersham Biosciences) with the following settings: PMT at 750 V, excitation at 495 nm, emission at 535 nm.

RESULTS

Domain Deletion Analysis. Classical bacterial NAD$^+$-dependent DNA ligases are composed of four distinct domains (*21*). Domain 1 consists of subdomain 1a and an adenylation domain (Figure 1A). Domain 2 is the OB-fold, a common oligonucleotide/oligosaccharide binding domain (*45*). Domain 3 contains a zinc finger motif and a subdomain consisting of four helix−hairpin−helix motifs. Domain 4 is the BRCT domain. The nucleotidyl transferase core encompasses the adenylation domain and much of the OB-fold (*21*). Since the domain architecture is well defined from the crystal structure of the *Thermus filiformis* NAD$^+$-dependent DNA ligase (*21*), we designed PCR primers that allowed us to delete domains at the interdomain regions. To investigate the functional role of various domains on NAD$^+$-dependent ligases, we constructed three domain deletion mutants by PCR. For the Δ584 mutant, we deleted domain 4 (BRCT domain); for the Δ429 mutant, we removed the BRCT domain, as well as the HhH subdomain of domain 3. The Δ406 mutant lacked both domains 3 and 4 (Figure 1A). The sites of deletion were chosen based on the alignment of the Tsp AK16D ligase and the *Tfi* ligase. All three domain deletion fragments were overexpressed in *E. coli* and purified as described in Experimental Procedures. The purified ligase proteins migrated normally on a SDS−PAGE gel (Figure 1B). To determine the ligation activity, a perfectly matched oligonucleotide substrate was assembled to form a nick (Figure 1C). Since one of the oligonucleotides is fluorescently labeled (Fam), the fluorescent ligation product (63 mer) can be distinguished from the unligated substrate (30 mer) on a GeneScan gel (Applied Biosystems). We initially assayed ligation activities of the three domain deletion mutants along with the wt Tsp AK16D ligase using enzyme (E)/substrate (S) ratio of 1:10 (E/S = 1:10, [S] = 10 nM). As shown in Figure 1D, while the wt ligase showed normal ligation activity on the nicked substrate, none of the deletion mutants showed detectable ligation product. Since domain deletion may substantially reduce ligation activity to below detection when the enzyme concentration was low, we increased the E/S ratio to 10:1 ([S] = 10 nM). As shown in Figure 1E, when the enzyme was in excess, ligation activity

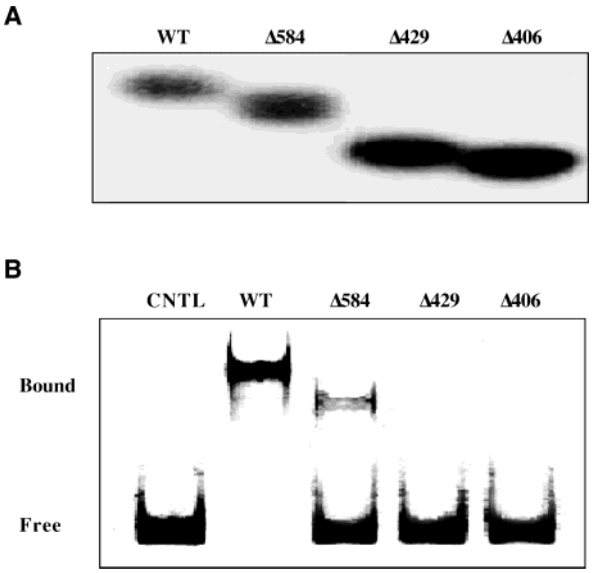

FIGURE 2: Adenylation and binding analysis of wt and mutant ligase. Panel A shows detection of adenylated wt ligase and deletion mutants. Ligase proteins (5 μM) were incubated with 0.5 mM [^{32}P]-NAD$^+$ in a reaction buffer, as detailed in Experimental Procedures, at 65 °C for 30 min. Adenylated ligase bands were visualized using a phosphorimager. Panel B shows gel mobility shift analysis of binding of wt and deletion mutant ligases to the nicked 3′ C/G substrate. Binding reactions containing the nicked C/G oligonucleotide substrate, 20 mM Tris-HCl (pH 7.6), 1 mM DTT, 15% glycerol, and 4 μM wt or mutant ligase protein were incubated at room temperature for 30 min prior to electrophoresis. CNTL denotes substrate control.

became detectable for Δ584 and Δ429. The yields of ligation product for Δ584 and Δ429 were 76% and 2%, respectively, as compared with that of the wt ligase. The very low but detectable ligation from Δ429 deletion mutant was not a result of spillover during sample loading on the GeneScan gel, since it was detectable even when the neighboring lanes were not used (data not shown).

Although these mutants have lost much of the ligation activity, it is possible that they still maintain enzyme adenylation activity (step 1). To examine this possibility, we measured formation of adenylated ligase using [^{32}P]-labeled NAD$^+$. All three deletion mutants were adenylated significantly (Figure 2A). Δ429, which lacked the BRCT domain and HhH subdomain, and Δ406, which lacked domains 3 and 4, still showed strong enzyme adenylation (Figure 2A). These results, consistent with previous studies on the *Bacillus stearothermophilus*, *Aquifex pyrophilus*, *Staphylococcus aureus*, *E. coli* LigB, and entomoxvirus ligases (*12*, *14*, *44*, *46*, *47*), suggest that the C-terminal domains 3 and 4 primarily affect ligation activity by causing defects at steps after step 1 (enzyme adenylation).

To assess the potential role of individual domains in DNA binding, we performed gel mobility shift analysis on these mutants (Figure 2B). The wt Tsp AK16D ligase formed a distinct retarded band. The retarded band generated by Δ584 was at most one-third as intense as the band generated by the wt ligase, suggesting that the BRCT domain plays a role in DNA binding (Figure 2B). As expected, the retarded band generated by Δ584 migrated slightly faster than the wt since Δ584 is a smaller protein. No retarded bands were detected in Δ429 or Δ406, suggesting that the HhH subdomain, and possibly the Zn finger motif, plays an important role in DNA

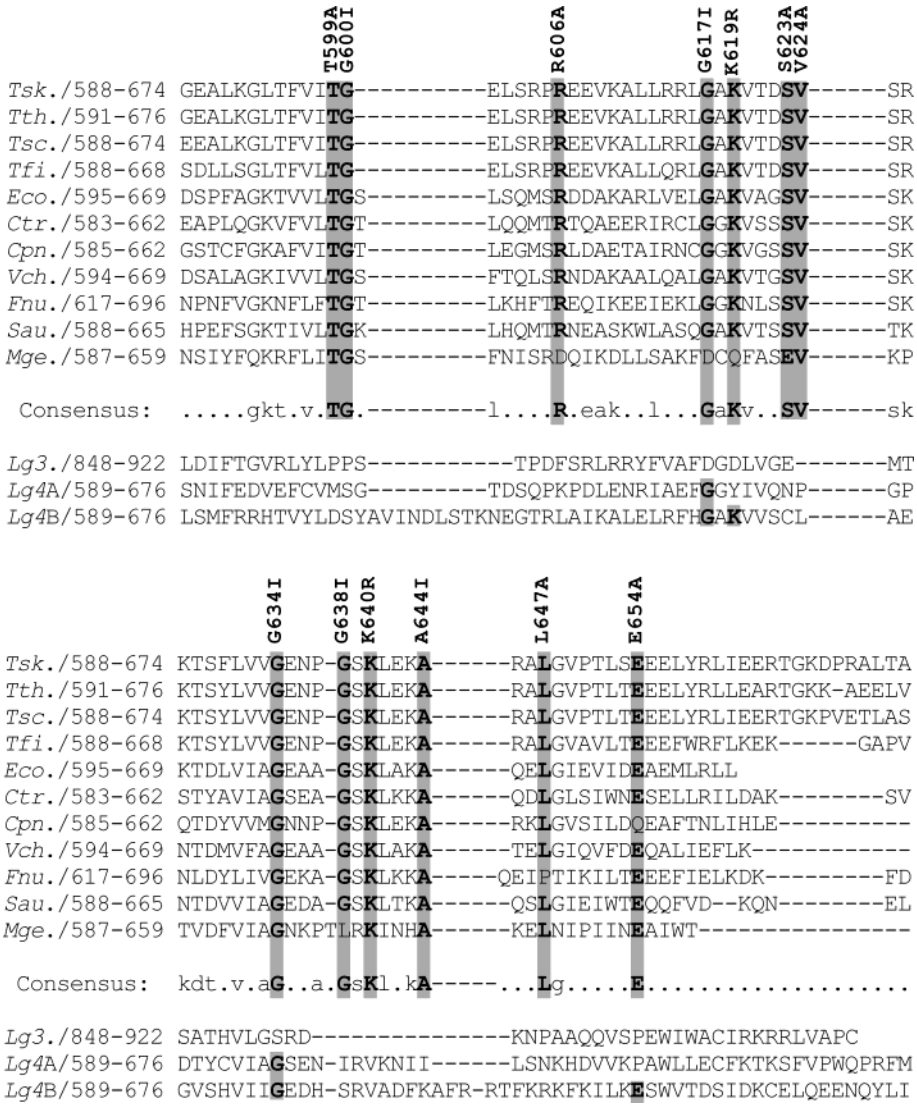

FIGURE 3: Representative sequence alignment of the BRCT domain in DNA ligases. Sequence alignment of NAD^+-dependent DNA ligases was initially performed using Multalin 5.4.1 (prodes.toulouse.inra.fr/multalin/, *58*) to determine an overall consensus sequence. The Sanger Institute's Pfam database (www.sanger.ac.uk/Software/Pfam/, *59*) was then used to selectively align the BRCT domain of the various ligases shown. Sites for mutation were chosen on the basis of 90% consensus. Genbank accession numbers are shown after the species names: *Tak*, *Thermus* sp. AK16D, 4235370; *Tth*, *Thermus thermophilus*, 118780; *Tsc*, *Thermus scotoductus*, 609276; *Tfi*, *Thermus filiformis*, 3800758; *Eco*, *Escherichia coli*, 146613; *Ctr*, *Chlamydia trachomatis*, 3328547; *Cpn*, *Chlamydophilia pneumoniae* CWL029, 4376415; *Vch*, *Vibrio cholerae*, 9655431; *Fnu*, *Fusobacterium nucleatum*, 19705308; *Sau*, *Staphylococcus aureus*, 1318294; *Mge*, *Mycoplasma genitalium*, 12045108; Lg4A and Lg4B, human DNA ligase IV, 1706482. Amino acid residues selected for site-directed mutagenesis are highlighted, and the resulting mutants are indicated.

binding in bacterial NAD^+-dependent ligases. These results are consistent with the notion that the C-terminal domains play a role in DNA binding, as demonstrated previously by gel shift analysis using various C-terminal deletion protein fragments (*44*, *46*, *47*).

Ligation Activity of 13 Site-Directed Mutants at the BRCT Domain. Given the significant effects of the BRCT domain deletion on ligation activity, we set out to identify amino acid residues at the BRCT domain that may be accountable for the substantial loss of ligation activity. Sixty sequences of the BRCT domain of the NAD^+-dependent ligases obtained from Genbank were aligned using Multalin. A representative alignment is shown in Figure 3. Thirteen highly conserved amino acid residues in NAD^+-dependent ligases were chosen for site-directed mutagenesis. Six mutants, T599, S623, V624, L647 and E654, were changed to alanine to remove the functional side chain. Two positively charged residues, K619 and K640, were substituted by arginine to maintain the positive charge. G600, G617, G634, G638, and A644 were switched to a bulkier isoleucine residue. Interestingly, G617 and G634 are also conserved in the two BRCT domains of human ATP-dependent ligase IV, and the position corresponding to G638 at the first BRCT domain of ligase IV is an isoleucine residue (Figure 3).

Site-directed mutagenesis was performed using the QuikChange kit (Stratagene), and all mutant sequences were doubly confirmed in cloning and expression vectors. All 13 mutants except G600I achieved significant overexpression after IPTG induction. G600I did not appear to express well, or may have been misfolded or degraded (Figure 4A). Therefore, no further studies were performed on this mutant. All other mutant proteins were quantified by SDS−PAGE analysis using BSA as a standard (Figure 4A).

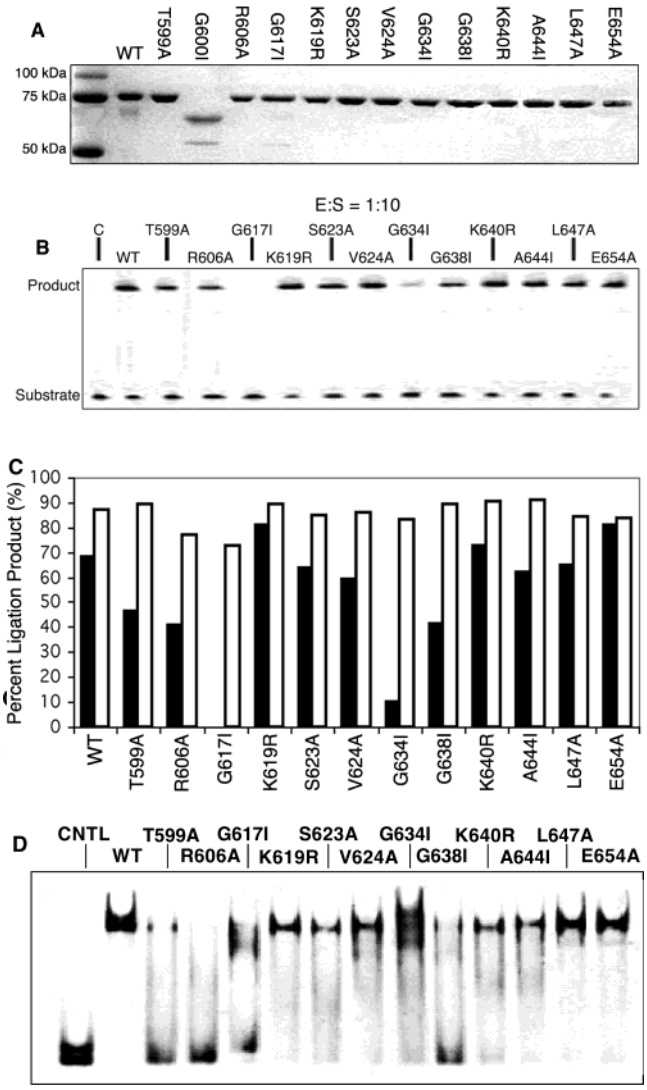

FIGURE 4: Analysis of 13 site-directed mutants at the BRCT domain. Panel A presents the SDS−PAGE analysis. Thirteen mutants were analyzed on a 15% SDS−PAGE gel and visualized with Coomassie brilliant blue staining. Panel B presents a representative ligation activity assay. Ligation assays were performed as described in Experimental Procedures with 1 nM ligase mutant and 10 nM nicked C/G substrate. C denotes substrate control. Panel C shows the quantitative analysis of ligation activity with 1 nM ligase mutant and 10 nM nicked C/G substrate (E/S = 1:10, solid bars) and 100 nM ligase mutant and 10 nM nicked C/G substrate (E/S = 10:1, open bars). Values represent an average of two independent experiments. Panel D shows the gel mobility shift analysis of binding of wt and deletion mutant ligases to the nicked 3′ C/G substrate. Binding reactions containing the nicked C/G oligonucleotide substrate, 20 mM Tris-HCl (pH 7.6), 1 mM DTT, 15% glycerol, and 4 μM wt or mutant ligase protein were incubated at room temperature for 30 min prior to electrophoresis. CNTL denotes substrate control.

With the nicked substrate in excess, K619R, S623A, V624A, K640R, A644I, L647A, and E654A showed comparable ligation activity with the wt ligase (Figure 4B,C, solid bars). Ligation yields from T599A, R606A, and G638I were about 30−40% lower than that from the wt ligase. G634I only achieved about 10% ligation as compared with about 70% by the wt ligase. Similar to the results obtained from the domain deletion mutants, G617I did not show any detectable ligation when the enzyme concentration was low (Figure 4B). To detect low level ligation activities, the E/S ratio was increased to 10:1. Under these conditions, all the mutants including G617I were able to achieve 70−80% ligation (Figure 4C, open bars).

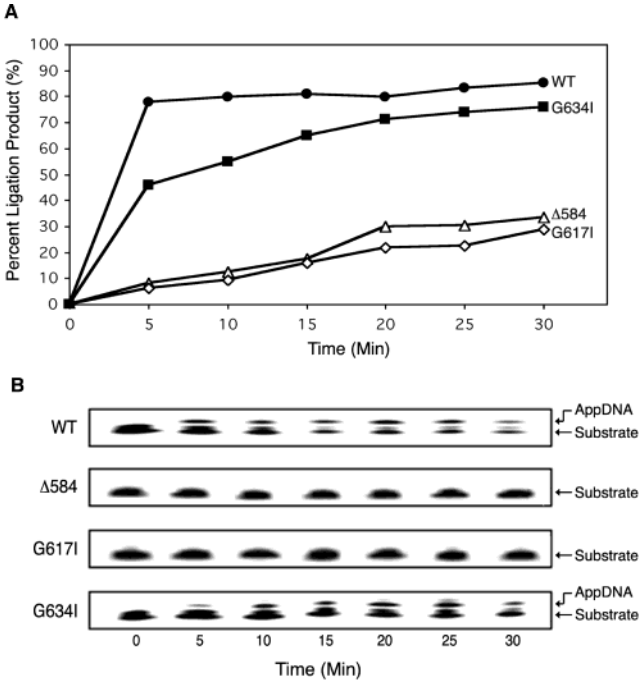

FIGURE 5: Time course analysis of Δ584, G617I, G634I, and the wt Tsp AK16D ligase. Panel A shows the time course analysis of ligation activities. The reaction mixtures containing 10 nM ligase enzyme, 10 nM nicked C/G substrate, and other components as described in Experimental Procedures were incubated at 65 °C for indicated times. Closed circles denote wt Tsp AK16D ligase; closed squares denote G634I; open triangles denote Δ584; open diamonds denote G617I. Data represents the average of two independent experiments. Panel B shows the accumulation of AppDNA over the time course. AppDNA denotes the AMP−DNA intermediate.

The effects of these site-directed mutations on DNA binding were evaluated by gel mobility shift analysis. The intensities of retarded bands were in general consistent with their ligation activities. Mutants that exhibited wt or close to wt level ligation activities (K619R, S623A, V624A, K640R, K644I, L647A, and E654A) showed distinct retarded bands with good binding affinity (Figure 5). T599A, R606A and G638I, which had reduced ligation activities (Figure 4C), showed much reduced binding (Figure 4D). The smearing effect seen in G634I, as well as other mutants, indicated that some of the mutant−DNA complexes may have experienced dissociation during gel electrophoresis. Although a diffused retarded band was detected in G617I, it migrated slightly faster than that generated by the wt ligase (Figure 4D). G634I appeared to generate three retarded bands with one corresponding to the location of the wt ligase−DNA complex and one above and one below. These results suggested that aberrant interactions occurring between G617I or G634I and DNA may contribute to the substantially lower ligation activities (Figure 4B,C).

To discern the potential similarity or difference among G617I, G634I, Δ584, and the wt ligase, we conducted a time course analysis under the conditions of E/S = 1:1 (Figure 5A). G634I showed a lower-than-wt activity during the initial 15 min and then started to approach the ligation level comparable to the wt enzyme. This kinetic behavior is in general consistent with the ligation activity observed with

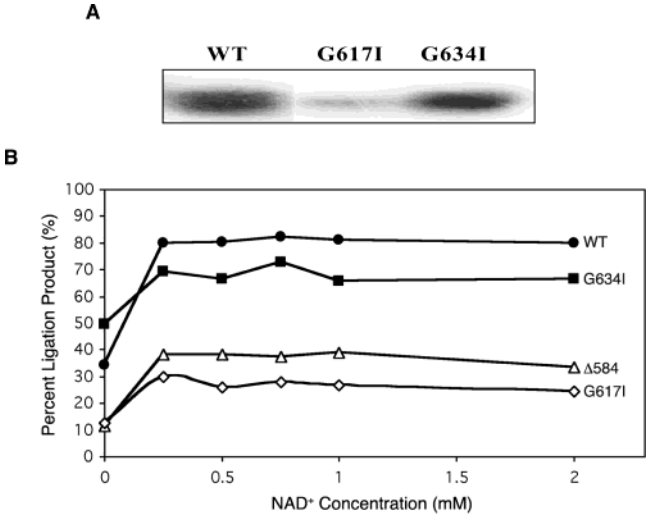

FIGURE 6: Effects of NAD^+ on ligation activity. Panel A shows enzyme adenylation. Ligase proteins (5 μM) were incubated with 0.5 mM [^{32}P]-NAD^+ in a reaction buffer as detailed in Experimental Procedures at 65 °C for 30 min. Adenylated ligase bands were visualized using a phosphorimager. Panel B shows titration of NAD^+ concentrations on ligation activity. The reaction mixtures containing 10 nM ligase, 10 nM nicked C/G substrate, and other components as described in Experimental Procedures were incubated at 65 °C for 30 min. Closed circles denote wt Tsp AK16D ligase; closed squares denote G634I; open triangles denote Δ584; open diamonds denote G617I. Data represents the average of two independent experiments.

E/S = 1:10 and E/S = 10:1 (Figure 4). Furthermore, both G634I and the wt ligase accumulated AMP−DNA intermediate (AppDNA) during the entire course of ligation reaction (Figure 5B). These results suggest that the nick closure step (step 3) is a rate-limiting event for both G634I and the wt ligase. However, there was a difference between the amount of the AppDNA intermediate accumulated during the course of the ligation reaction. The most significant difference occurred in the first 15 min. While the ratio of AppDNA and unligated substrate reached about 50% for the wt ligase, the level of AppDNA remained at about 25% for G634I (Figure 5B, 15 min), indicating a defect at the substrate adenylation step (step 2) for the latter.

On the other hand, both G617I and the Δ584 deletion mutant showed a comparable low ligation activity throughout the entire time course analysis (Figure 5A). In addition, neither G617 nor Δ584 appeared to accumulate AppDNA during the reaction (Figure 5B), suggesting that the mutational effects on ligation function by an isoleucine substitution at the G617 position were similar to the deletion of the entire BRCT domain as seen in Δ584. Under these assay conditions, the ligation activities demonstrated by G617I and Δ584 were less than half than those demonstrated by G634I and the wt ligase (Figure 5A).

Effects of NAD^+ on Ligation Activity. To determine the effects of the G617I and G634I substitutions may have on step 1, we examined formation of adenylated ligase using [^{32}P]-labeled NAD^+. Both G617I and G634I remained capable of forming the AMP−ligase intermediate (Figure 6A). However, G617I appeared to be only weakly adenylated.

Although the KXDG adenylation motif (motif I) is located at the N-terminal part of the ligase based on structural and biochemical analysis (Figure 1A) (*3*, *15*, *21*), the BRCT domain seemed to affect the enzyme adenylation step as well (*46*). We then determined ligation activities of G617I, Δ584, G634, and the wt ligase at different NAD^+ concentrations (Figure 6B). Without supplementing exogenous NAD^+, all of them still showed significant ligation activity (Figure 6B, 0 mM NAD^+). These results suggest that a certain portion of the mutants and the wt ligase have been adenylated in vivo, which can complete steps 2 and 3 without input of NAD^+. The degree of the in vivo adenylation appeared to be higher in G634I and the wt ligase (Figure 5B). With increasing NAD^+ concentrations, both G634I and the wt ligase converted most of the substrate to ligation product. On the other hand, input of increasing NAD^+ only had a limited enhancement effect for G617I and Δ584. The ligation yields remained below 30% and 40% for G617I and Δ584, respectively (Figure 6B).

Ligation of Mismatched Substrates. With the exception of G617I and G634I, all other mutants still maintained at least 50% level of wt ligation activity on the perfectly matched nick substrate (Figure 4B,C). Given the significant effects observed on BRCT domain deletion (Δ584) and some site-directed mutations, their ligation activities on mismatched substrates may change due to amino acid substitutions. To investigate this possibility, we measured ligation yields of 10 mutants using nick substrates with a 3′ mismatch at the penultimate position or the nick junction. After 60 min incubation, the wt ligase yielded 40% 3′-penultimate misligation product (Figure 7A,B). Under the same reaction conditions, G638I generated about twice as much 3′-penultimate misligation product as the wt ligase. To further confirm the results, a time course analysis was conducted on G638I, K619R, and the wt ligase. The wt ligase showed a steady increase over a 60-min period to reach about 40% ligation product (Figure 7C). G638I, on the other hand, readily reached 70% ligation within 10 min on the 3′-penultimate substrate and plateau to about 80% (Figure 7C). In fact, the ligation kinetics of G638I on the 3′-penultimate mismatched substrate is similar to the wt ligase on a perfectly matched substrate (Figures 5A and 7C). Although both the wt ligase and all mutants accumulated the AppDNA intermediate, most of the intermediate generated by G638I was converted to the ligation product (Figure 7A, compare G638I lane with others). These results indicate that G638I exhibits a greater ligation on the 3′-penultmate mismatched substrate by accelerating the nick closure step. Some mutants such as T599A showed some enhancement in ligation fidelity (Figure 7A,B).

The mismatch ligation pattern obtained from the 10 mutants using the nick substrate with a 3′ mismatch at the nick junction was very similar to the results obtained from the 3′-penultimate mismatched substrate (Figure 8A). G638I again showed a 2-fold greater ligation in comparison with the wt ligase, which was further confirmed by a time course analysis (Figure 8B,C).

DISCUSSION

NAD^+-dependent DNA ligases are multidomain proteins (*21*). The primary objective of this study is to investigate the role of the BRCT domain in ligation function. All classic bacterial NAD^+-dependent ligases contain a BRCT domain

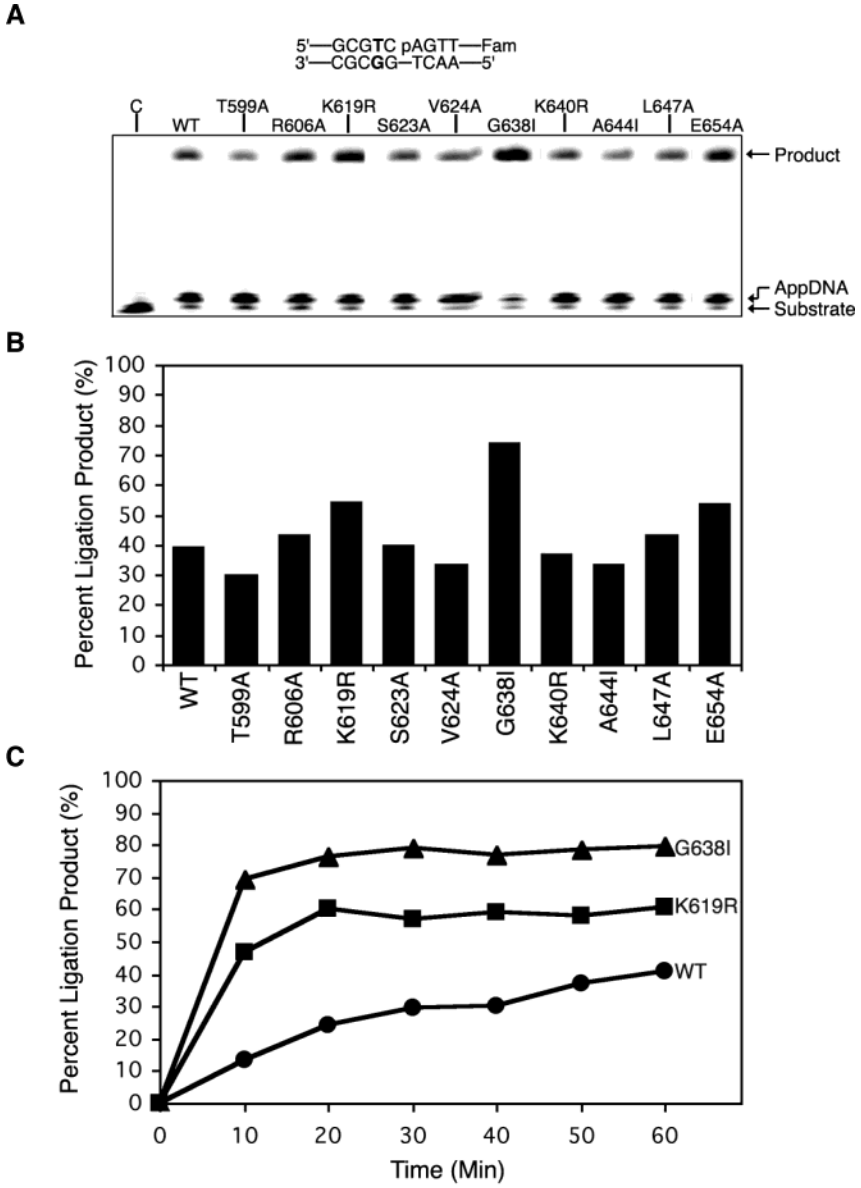

FIGURE 7: Effects of site-directed mutations on ligation fidelity of 3′-penultimate T/G mismatch substrate. Panel A presents a representative ligation assay chromatogram. The reaction mixtures containing 10 nM ligase, 10 nM 3′-penultimate T/G mismatched nicked substrate, and other components as described in Experimental Procedures were incubated at 65 °C for 60 min and analyzed on a 10% GeneScan gel. C denotes substrate control. AppDNA denotes AMP−DNA intermediate. Panel B presents the quantitative analysis of ligation product. Panel C presents the time course analysis of ligation activity of 3′-penultimate T/G mismatch substrate. Assays were performed as described in panel A except that reactions were stopped at indicated time points. Closed circles denote wt Tsp AK16D ligase; closed squares denote K619R; closed triangles denote G638I. Results represent the average of two independent experiments.

with the exception of a few bacteria that contain additional NAD+-dependent ligases. This work demonstrates that the BRCT domain plays an important role in NAD+-dependent ligases. Deletion of the BRCT domain (Δ584) renders the ligation activity undetectable when the E/S ratio is 1:10 (Figure 1D). The Δ584 mutant shows only a low ligation activity even when the E/S ratio is increased to 1:1 (Figure 5A). When the HhH subdomain or the entire domain 3 is deleted in addition to the BRCT domain as seen in Δ429 and Δ406, the ligase fragments are essentially inactive, indicating the pivotal role of the C-terminal domains in NAD+-dependent ligases (Figure 1). Consistent with previous deletion studies (*44*, *46*, *47*), domains 3 and 4 are not essential for enzyme adenylation in step 1 (Figure 2). The BRCT domain can mediate protein−protein interactions, as well as DNA binding (*26*, *27*, *35*). Both HhH motifs and Zn fingers are known for their role in protein−DNA interactions (*18*, *48*, *49*). Previous studies on *Bst*, *Apy*, and *Sau* ligases have implicated the involvement of C-terminal domains in DNA binding (*44*, *46*, *47*). The well-defined domain organization in the *Tfi* ligase crystal structure allowed us to construct domain deletion mutants. Data obtained from ligation and DNA binding analysis of Tsp AK16D ligase indicates that the BRCT domain and the HhH subdomain play an important role in DNA binding.

The focus of this work is to identify conserved amino acid residues at the BRCT domain that are important for ligase function and their effects on different steps of DNA ligation. Thirteen conserved amino acid residues were mutated by site-directed mutagenesis (Figures 3−4). G600, conserved in all 60 NAD+-dependent ligases, is located downstream to a highly hydrophobic region in the BRCT domain (Figure 3)

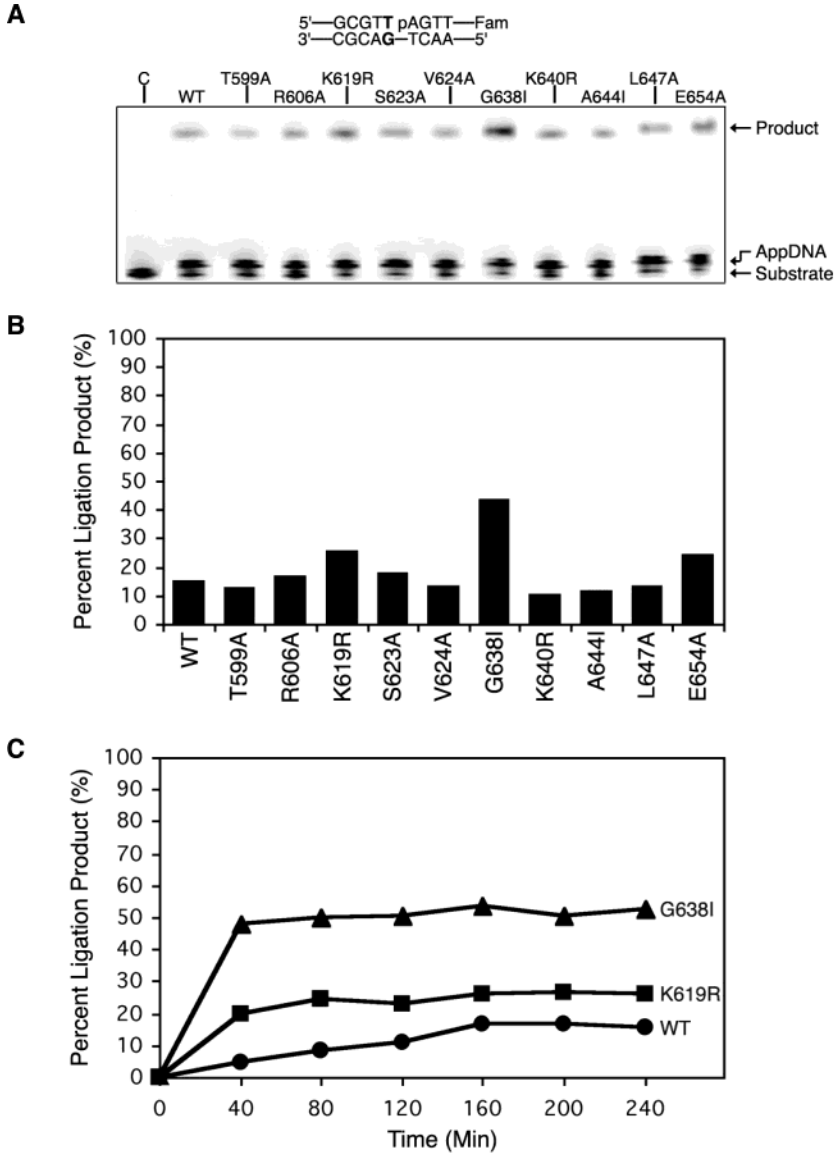

FIGURE 8: Effects of site-directed mutation on ligation fidelity of 3′ T/G mismatch substrate (3′ pT/G). Panel A presents a representative ligation assay chromatogram. The reaction mixtures containing 10 nM ligase, 10 nM 3′ T/G mismatched nicked substrate, and other components as described in Experimental Procedures were incubated at 65 °C for 60 min and analyzed on a 10% GeneScan gel. C denotes substrate control. AppDNA denotes AMP−DNA intermediate. Panel B presents the quantitative analysis of ligation product. Panel C presents the time course analysis of ligation activity of 3′ T/G mismatch substrate. Assays were performed as described in panel A except that reactions were stopped at indicated time points. Closed circles denote wt Tsp AK16D ligase; closed squares denote K619R; closed triangles denote G638I. Results represent the average of two independent experiments.

(*25*). Apparently, G600 may be important for maintaining the ligase structure, because G600I did not seem to express well in *E. coli*.

In many ways, the G617I ligase mutant behaves similarly to the Δ584 BRCT domain deletion mutant. First, both G617I and Δ584 fail to ligate the matched substrate with the E/S ratio of 1:10 (Figures 1D and 4B). Second, neither Δ584 nor G617I binds to nicked DNA as tightly as the wt ligase (Figures 2B and 4D). Third, both of the mutants show similar kinetics on the matched substrate ligation (Figure 5A). Fourth, unlike the wt ligase, both of the mutants do not accumulate the AppDNA intermediate (Figure 5B). Finally, both of mutants respond to NAD^+ titration in a similar fashion (Figure 6B). These results suggest that the deleterious effects on ligation function caused by G617I point mutation to a large extent are comparable with deletion of the entire BRCT domain.

Since no detectable AppDNA intermediate accumulation was observed in G617I and Δ584 (Figure 5B), the major defect caused by glycine to isoleucine substitution at position 617 or deletion of the entire BRCT domain (Δ584) is likely to occur at step 1 (enzyme adenylation) or step 2 (substrate adenylation). For Δ584, the effects on ligation may primarily lie at step 2 since it forms AMP−ligase to the level similar to that of the wt ligase (Figure 2). The weaker binding of Δ584 to DNA may contribute to its effect on step 2. For G617I, it appears that step 1 is significantly affected (Figure 6A), resulting in weak enzyme adenylation. G617I may have adopted a slightly different conformation, which inhibits its adenylation and causes aberrant migration as seen in gel mobility shift analysis.

The G634I substitution substantially reduces ligation activity, yet in many aspects, this mutant behaves similarly to the wt ligase (Figures 4B, 5, and 6). The enzyme

adenylation step (step 1) does not seem to be affected by the G634I substitution (Figure 6A). The major difference between G634I and the wt enzyme is that the former appears slower in substrate adenylation (step 2), resulting in reduced accumulation of AppDNA in comparison with the wt ligase (Figure 5B). Thus, like the BRCT domain deletion mutant, G634I may primarily affect the substrate adenylation (step 2). The aberrant migration observed in gel mobility shift analysis may contribute to the effect of G634I on step 2. It is worth noting that both BRCT domains in human ligase IV encode a glycine residue in the corresponding positions (Figure 3). It will be interesting to test the mutational effects that these two glycine residues may have on human ligase IV.

The G638I substitution increases ligation of mismatched substrates by at least 2-fold (Figures 7 and 8). The major rate enhancement appears to occur at the nick closure step (step 3), which results in greater conversion of the AppDNA to the ligation product (Figure 7A). These results suggest that the BRCT domain in NAD^+ ligases not only plays a role in step 1 or 2 but also may play a role in step 3. We have not detected increased binding affinity of G638I to nicked mismatch substrates (data not shown). Thus, the greater mismatch ligation may not be attributed to a binding effect. The ability of a ligase to discriminate a mismatched substrate is regulated at both steps 2 and 3 (*41*, *50*). G638I appears to lower its ligation fidelity by enhancing nick closure. It is interesting to note that the corresponding position at the first BRCT domain of the more promiscuous human ligase IV is an isoleucine residue (Figure 3). In the past, engineering of higher fidelity ligases primarily focuses on the nucleotidyl transferase core (*16*). Data obtained from this study indicate that the BRCT domain also plays a role in modulating ligation fidelity. Therefore, rational or random mutagenesis at the BRCT domain may generate ligases with desired fidelity.

The BRCT domain in NAD^+ ligases appears to be very flexible in the open conformation based on the crystal structures of the *Tfi* ligase (*21*). In the closed conformation, domain 3 is shifted by ~6.4 Å toward domain 1, bringing the BRCT domain in close proximity to helix B of subdomain 1a (Figure 1). Subdomain 1a is essential for the interaction between NAD^+ and the ligase (*51*). It is proposed that during the course of ligation, NAD^+ ligase experiences runs of open and closed conformations during enzyme adenylation, substrate adenylation, and nick closure (*5*). The potential interactions between the BRCT domain and subdomain 1a may act as a gate to regulate DNA binding and release or form a sliding clamp-like structure to facilitate sliding on DNA (*5*). Recent conformational analyses of *E. coli* and *Thermus scotoductus* NAD^+ ligases have led to a model in which the adenylation-dependent open−close conformational change induces the ligase to a catalytically activated state (*52*, *53*). Similar open−close models are proposed for T7 ligase, T4 ATP ligase, and mRNA capping enzyme (*17*, *54*−*56*).

Although our data do not provide direct evidence to prove or disprove the potential protein−protein interactions proposed on the basis of *Tfi* ligase structure, they are consistent with this model. Previous studies indicate that a small C-terminal fragment of T7 ATP-dependent ligase can stimulate the enzyme adenylation of a large N-terminal domain (*57*). However, a small C-terminal fragment (aa 398−670) of *Bst* NAD^+-dependent ligase cannot stimulate the enzyme adenylation of a large N-terminal domain (aa 1−318) (47). It is possible that a full-length protein is required to coordinate the potential protein−protein interactions in bacterial NAD^+-dependent ligase. G617 in Tsp AK16D ligase is located in the region that potentially interacts with the subdomain 1a. If this interaction is important for enzyme adenyalion (step 1) or substrate adenylation (step 2), it is conceivable that disruption of this potential interaction by deletion of the BRCT domain (Δ584) or G617I substitution may severely impede these ligation functions. Deletion of the BRCT domain may completely abolish such an interaction, affecting substrate adenylation at step 2, yet without exerting much influence on step 1 (enzyme adenylation). The G617I substitution may effect an aberrant interaction between BRCT domain and domain 1 as demonstrated by gel mobility shift analysis, resulting in impediment of enzyme adenylation by domain 1. The effect G634I exhibits on the substrate adenylation step and the acceleration of nick closure step on mismatched substrates by G638I may also be mediated through the potential interactions between the BRCT domain and the subdomain 1a. As a consequence, these interactions may modulate DNA binding, catalysis or both in step 2 or 3. It is also possible that the influence on step 2 or 3 exhibited by G634I or G638I is largely a local effect confined the BRCT domain itself. In summary, this biochemical analysis reveals the conserved amino acids at the BRCT domain that play an important functional role in the three steps of DNA ligation.

ACKNOWLEDGMENT

We thank Drs. Francis Barany, Don Bergstrom, Alan Friedman, and other members of the Cao lab for discussions. We also thank Thomas Hitchcock for critically reading the manuscript.

REFERENCES

1. Lehman, I. R. (1974) DNA ligase: structure, mechanism, and function, *Science 186*, 790−797.
2. Cao, W. (2002) DNA Ligases: Structure, Function, and Mechanism, *Curr. Org. Chem. 6*, 827−839.
3. Sriskanda, V., Schwer, B., Ho, C. K., and Shuman, S. (1999) Mutational analysis of *Escherichia coli* DNA ligase identifies amino acids required for nick-ligation in vitro and for in vivo complementation of the growth of yeast cells deleted for CDC9 and LIG4, *Nucleic Acids Res. 27*, 3953−3963.
4. Aravind, L., and Koonin, E. V. (1999) Gleaning nontrivial structural, functional and evolutionary information about proteins by iterative database searches, *J. Mol. Biol. 287*, 1023−1040.
5. Doherty, A. J., and Suh, S. W. (2000) Structural and mechanistic conservation in DNA ligases, *Nucleic Acids Res. 28*, 4051−4058.
6. Odell, M., Malinina, L., Sriskanda, V., Teplova, M., and Shuman, S. (2003) Analysis of the DNA joining repertoire of Chlorella virus DNA ligase and a new crystal structure of the ligase-adenylate intermediate, *Nucleic Acids Res. 31*, 5090−5100.
7. Sawaya, R., and Shuman, S. (2003) Mutational analysis of the guanylyltransferase component of Mammalian mRNA capping enzyme, *Biochemistry 42*, 8240−8249.
8. Wang, L. K., Ho, C. K., Pei, Y., and Shuman, S. (2003) Mutational analysis of bacteriophage T4 RNA ligase 1. Different functional groups are required for the nucleotidyl transfer and phosphodiester bond formation steps of the ligation reaction, *J. Biol. Chem. 278*, 29454−29462.
9. Yin, S., Ho, C. K., and Shuman, S. (2003) Structure−function analysis of T4 RNA ligase 2, *J. Biol. Chem. 278*, 17601−17608.

10. Sriskanda, V., and Shuman, S. (2002) Role of nucleotidyltransferase motifs I, III and IV in the catalysis of phosphodiester bond formation by Chlorella virus DNA ligase, *Nucleic Acids Res. 30*, 903−911.
11. Sriskanda, V., and Shuman, S. (2002) Role of nucleotidyl transferase motif V in strand joining by chlorella virus DNA ligase, *J. Biol. Chem. 277*, 9661−9667.
12. Sriskanda, V., Moyer, R. W., and Shuman, S. (2001) NAD+-dependent DNA ligase encoded by a eukaryotic virus, *J. Biol. Chem. 276*, 36100−36109.
13. Sriskanda, V., Kelman, Z., Hurwitz, J., and Shuman, S. (2000) Characterization of an ATP-dependent DNA ligase from the thermophilic archaeon Methanobacterium thermoautotrophicum, *Nucleic Acids Res. 28*, 2221−2228.
14. Sriskanda, V., and Shuman, S. (2001) A second NAD(+)-dependent DNA ligase (LigB) in *Escherichia coli*, *Nucleic Acids Res. 29*, 4930−4934.
15. Luo, J., and Barany, F. (1996) Identification of essential residues in Thermus thermophilus DNA ligase, *Nucleic Acids Res. 24*, 3079−3085.
16. Luo, J., Bergstrom, D. E., and Barany, F. (1996) Improving the fidelity of *Thermus thermophilus* DNA ligase, *Nucleic Acids Res. 24*, 3071−3078.
17. Doherty, A. J., and Dafforn, T. R. (2000) Nick recognition by DNA ligases, *J. Mol. Biol. 296*, 43−56.
18. Sriskanda, V., and Shuman, S. (1998) Mutational analysis of Chlorella virus DNA ligase: catalytic roles of domain I and motif VI, *Nucleic Acids Res. 26*, 4618−4625.
19. Subramanya, H. S., Doherty, A. J., Ashford, S. R., and Wigley, D. B. (1996) Crystal structure of an ATP-dependent DNA ligase from bacteriophage T7, *Cell 85*, 607−615.
20. Singleton, M. R., Hakansson, K., Timson, D. J., and Wigley, D. B. (1999) Structure of the adenylation domain of an NAD+-dependent DNA ligase, *Structure 7*, 35−42.
21. Lee, J. Y., Chang, C., Song, H. K., Moon, J., Yang, J. K., Kim, H.-K., Kwon, S.-T., and Suh, S. W. (2000) Crystal structure of NAD+-dependent DNA ligase: modular architecture and functional implications, *EMBO J. 19*, 1119−1129.
22. Wang, Y. C., Burkhart, W. A., Mackey, Z. B., Moyer, M. B., Ramos, W., Husain, I., Chen, J., Besterman, J. M., and Tomkinson, A. E. (1994) Mammalian DNA ligase II is highly homologous with vaccinia DNA ligase. Identification of the DNA ligase II active site for enzyme-adenylate formation, *J. Biol. Chem. 269*, 31923−31928.
23. Tomkinson, A. E., Totty, N. F., Ginsburg, M., and Lindahl, T. (1991) Location of the active site for enzyme-adenylate formation in DNA ligases, *Proc. Natl. Acad. Sci. U.S.A. 88*, 400−404.
24. Tomkinson, A. E., Lasko, D. D., Daly, G., and Lindahl, T. (1990) Mammalian DNA ligases. Catalytic domain and size of DNA ligase I, *J. Biol. Chem. 265*, 12611−12617.
25. Bork, P., Hofmann, K., Bucher, P., Neuwald, A. F., Altschul, S. F., and Koonin, E. V. (1997) A superfamily of conserved domains in DNA damage-responsive cell cycle checkpoint proteins, *FASEB J. 11*, 68−76.
26. Callebaut, I., and Mornon, J. P. (1997) From BRCA1 to RAP1: a widespread BRCT module closely associated with DNA repair, *FEBS Lett. 400*, 25−30.
27. Zhang, X., Morera, S., Bates, P. A., Whitehead, P. C., Coffer, A. I., Hainbucher, K., Nash, R. A., Sternberg, M. J., Lindahl, T., and Freemont, P. S. (1998) Structure of an XRCC1 BRCT domain: a new protein−protein interaction module, *EMBO J. 17*, 6404−6411.
28. Chai, Y. L., Cui, J., Shao, N., Shyam, E., Reddy, P., and Rao, V. N. (1999) The second BRCT domain of BRCA1 proteins interacts with p53 and stimulates transcription from the p21WAF1/CIP1 promoter, *Oncogene 18*, 263−268.
29. Soulier, J., and Lowndes, N. F. (1999) The BRCT domain of the S. cerevisiae checkpoint protein Rad9 mediates a Rad9-Rad9 interaction after DNA damage, *Curr. Biol. 9*, 551−554.
30. Dulic, A., Bates, P. A., Zhang, X., Martin, S. R., Freemont, P. S., Lindahl, T., and Barnes, D. E. (2001) BRCT domain interactions in the heterodimeric DNA repair protein XRCC1-DNA ligase III, *Biochemistry 40*, 5906−5913.
31. Moore, D. J., Taylor, R. M., Clements, P., and Caldecott, K. W. (2000) Mutation of a BRCT domain selectively disrupts DNA single-strand break repair in noncycling Chinese hamster ovary cells, *Proc. Natl. Acad. Sci. U.S.A. 97*, 13649−13654.
32. Taylor, R. M., Moore, D. J., Whitehouse, J., Johnson, P., and Caldecott, K. W. (2000) A cell cycle-specific requirement for the XRCC1 BRCT II domain during mammalian DNA strand break repair, *Mol. Cell. Biol. 20*, 735−740.
33. Krishnan, V. V., Thornton, K. H., Thelen, M. P., and Cosman, M. (2001) Solution structure and backbone dynamics of the human DNA ligase IIIalpha BRCT domain, *Biochemistry 40*, 13158−13166.
34. Yamane, K., and Tsuruo, T. (1999) Conserved BRCT regions of TopBP1 and of the tumor suppressor BRCA1 bind strand breaks and termini of DNA, *Oncogene 18*, 5194−5203.
35. Yamane, K., Katayama, E., and Tsuruo, T. (2000) The BRCT Regions of Tumor Suppressor BRCA1 and of XRCC1 Show DNA End Binding Activity with a Multimerizing Feature, *Biochem. Biophys. Res. Commun. 279*, 678−684.
36. Yamane, K., Katayama, E., Sugasawa, K., and Tsuruo, T. (2000) Retinoblastoma susceptibility protein, Rb, possesses multiple BRCT-Ws, BRCA1 carboxyl-terminus-related W regions with DNA break-binding activity, *Oncogene 19*, 1982−1991.
37. Yu, X., Chini, C. C., He, M., Mer, G., and Chen, J. (2003) The BRCT domain is a phospho-protein binding domain, *Science 302*, 639−642.
38. Manke, I. A., Lowery, D. M., Nguyen, A., and Yaffe, M. B. (2003) BRCT repeats as phosphopeptide-binding modules involved in protein targeting, *Science 302*, 636−639.
39. Tomkinson, A. E., and Mackey, Z. B. (1998) Structure and function of mammalian DNA ligases, *Mutat. Res. 407*, 1−9.
40. Taylor, R. M., Wickstead, B., Cronin, S., and Caldecott, K. W. (1998) Role of a BRCT domain in the interaction of DNA ligase III-alpha with the DNA repair protein XRCC1, *Curr. Biol. 8*, 877−880.
41. Tong, J., Cao, W., and Barany, F. (1999) Biochemical properties of a high fidelity DNA ligase from *Thermus* species AK16D, *Nucleic Acids Res. 27*, 788−794.
42. Huang, J., Lu, J., Barany, F., and Cao, W. (2001) Multiple Cleavage Activities of Endonuclease V from Thermotoga maritima: Recognition and Strand Nicking Mechanism, *Biochemistry 40*, 8738−8748.
43. Chung, C. T., Niemela, S. L., and Miller, R. H. (1989) One-step preparation of competent *Escherichia coli*: transformation and storage of bacterial cells in the same solution, *Proc. Natl. Acad Sci. U.S.A. 86*, 2172−2175.
44. Kaczmarek, F. S., Zaniewski, R. P., Gootz, T. D., Danley, D. E., Mansour, M. N., Griffor, M., Kamath, A. V., Cronan, M., Mueller, J., Sun, D., Martin, P. K., Benton, B., McDowell, L., Biek, D., and Schmid, M. B. (2001) Cloning and functional characterization of an NAD(+)-dependent DNA ligase from *Staphylococcus aureus*, *J. Bacteriol. 183*, 3016−3024.
45. Murzin, A. G. (1993) OB(oligonucleotide/oligosaccharide binding)-fold: common structural and functional solution for nonhomologous sequences, *EMBO J. 12*, 861−867.
46. Lim, J. H., Choi, J., Kim, W., Ahn, B. Y., and Han, Y. S. (2001) Mutational analyses of *Aquifex pyrophilus* DNA ligase define essential domains for self-adenylation and DNA binding activity, *Arch. Biochem. Biophys. 388*, 253−260.
47. Timson, D. J., and Wigley, D. B. (1999) Functional domains of an NAD+-dependent DNA ligase, *J. Mol. Biol. 285*, 73−83.
48. Laity, J. H., Lee, B. M., and Wright, P. E. (2001) Zinc finger proteins: new insights into structural and functional diversity, *Curr. Opin. Struct. Biol. 11*, 39−46.
49. Doherty, A. J., Serpell, L. C., and Ponting, C. P. (1996) The helix-hairpin-helix DNA-binding motif: a structural basis for non-sequence-specific recognition of DNA, *Nucleic Acids Res. 24*, 2488−2497.
50. Tong, J., Barany, F., and Cao, W. (2000) Ligation Reaction Specificities of an NAD+-dependent DNA Ligase from Hyperthermophile *Aquifex aeolicus*, *Nucleic Acids Res. 28*, 1447−1454.
51. Sriskanda, V., and Shuman, S. (2002) Conserved residues in domain Ia are required for the reaction of *Escherichia coli* DNA ligase with NAD+, *J. Biol. Chem. 277*, 9695−9700.
52. Georlette, D., Blaise, V., Dohmen, C., Bouillenne, F., Damien, B., Depiereux, E., Gerday, C., Uversky, V. N., and Feller, G. (2003) Cofactor binding modulates the conformational stabilities and unfolding patterns of NAD(+)-dependent DNA ligases from *Escherichia coli* and *Thermus scotoductus*, *J. Biol. Chem. 278*, 49945−49953.
53. Georlette, D., Blaise, V., Bouillenne, F., Damien, B., Thorbjarnardottir, S. H., Depiereux, E., Gerday, C., Uversky, V. N., and Feller, G. (2004) Adenylation-dependent conformation and unfolding pathways of the NAD+-dependent DNA ligase from the thermophile *Thermus scotoductus*, *Biophys. J. 86*, 1089−1104.

54. Cherepanov, A. V., and de Vries, S. (2002) Dynamic mechanism of nick recognition by DNA ligase, *Eur. J. Biochem. 269*, 5993−5999.
55. Hakansson, K., and Wigley, D. B. (1998) Structure of a complex between a cap analogue and mRNA guanylyl transferase demonstrates the structural chemistry of RNA capping, *Proc. Natl. Acad Sci. U.S.A. 95*, 1505−1510.
56. Hakansson, K., Doherty, A. J., Shuman, S., and Wigley, D. B. (1997) X-ray crystallography reveals a large conformational change during guanyl transfer by mRNA capping enzymes, *Cell 89*, 545−553.
57. Doherty, A. J., and Wigley, D. B. (1999) Functional domains of an ATP-dependent DNA ligase, *J. Mol. Biol. 285*, 63−71.
58. Corpet, F. (1988) Multiple sequence alignment with hierarchical clustering, *Nucleic Acids Res. 16*, 10881−10890.
59. Bateman, A., Birney, E., Cerruti, L., Durbin, R., Etwiller, L., Eddy, S. R., Griffiths-Jones, S., Howe, K. L., Marshall, M., and Sonnhammer, E. L. (2002) The Pfam protein families database, *Nucleic Acids Res. 30*, 276−280.

BI049451C